Cleavage of the RNA polymerase II general transcription factor TFIIB tunes transcription during stress

Leah Gulyas,[1] Azra Lari,[1*] Sahil B. Shah,[2*] and Britt A. Glaunsinger[1,3,4]

[1]Department of Plant and Microbial Biology, University of California, Berkeley, CA 94720, USA
[2]Center for Computational Biology, University of California, Berkeley, Berkeley, CA, USA
[3]Department of Molecular and Cell Biology, University of California, Berkeley, CA 94720, USA
[4]Howard Hughes Medical Institute, University of California, Berkeley, CA 94709, USA

*Authors contributed equally to this work

Abstract

Cellular stressors often cause widespread repression of RNA polymerase II (RNAP II) activity, which is thought to facilitate a focused transcriptional output towards stress resolution. In many cases, however, the underlying regulatory mechanisms remain unknown. Here, we demonstrate that stress-induced downregulation of the general transcription factor TFIIB tunes the expression of specific stress response genes. In response to a variety of stressors, TFIIB is proteolytically cleaved at a conserved aspartic acid residue by caspases 3 and 7. Using both overexpression and endogenous base-editing, we find that B and T cells that are unable to cleave TFIIB fail to appropriately dampen transcription of short, stimulus-responsive and proto-oncogenic genes. The promoters of TFIIB-sensitive genes are bound by TFIIB and RNAP II, although their transcription is restrained until stimulated by stress. Subsequently, their expression is modulated through TFIIB cleavage. We further demonstrate that stress-induced TFIIB cleavage prevents aberrant lymphocyte proliferation and suppresses transcription from a pathogenic gammaherpesvirus. Hence, caspase targeting of TFIIB destabilizes transcription to tune gene expression, allowing for proper stress resolution.

Introduction

Cell stress is accompanied by rapid changes to the transcriptome. This involves the induction of genes required for stress resolution, but is also frequently associated with broad downregulation of basal gene expression by RNA polymerase II (RNAP II)

24 (Gulyas and Glaunsinger 2022). Suppression of RNAP II activity occurs during a variety
25 of stressors, including DNA damage (Tufegdžić Vidaković et al. 2020), hyperosmotic
26 stress (Rosa-Mercado et al. 2021), pro-apoptotic signals (Duncan-Lewis et al. 2021),
27 and viral infection (Abernathy et al. 2015; Bauer et al. 2018). Transcriptional repression
28 may focus gene expression on the stress response by freeing resources, as well as
29 restricting viral access to essential transcription machinery and/or permitting cells to
30 properly execute cell death pathways. While some drivers of stress-induced
31 transcriptional repression have been well studied, in many cases the underlying
32 mechanisms remain unknown. We previously found that transcriptional repression in
33 gammaherpesvirus-infected cells is coincident with reduced protein abundance of some
34 RNAP II machinery, most prominently the general transcription factor TFIIB (Hartenian
35 et al. 2020).
36
37 TFIIB is crucial for RNAP II recruitment and initiation. It stabilizes the general
38 transcription factor TFIID on promoter DNA, and its N-terminal B-ribbon threads to the
39 RNAP II core complex, drawing it to the promoter (Deng and Roberts 2007; Kostrewa et
40 al. 2009). TFIIB promoter binding is transient, with rapid dissociation and reassociation
41 observed *in vitro* (Zhang et al. 2016). Once stably bound, TFIIB assists RNAP II in
42 unwinding DNA and identifying the transcription start site (Kostrewa et al. 2009;
43 Sainsbury et al. 2013). TFIIB also has a more enigmatic role in 3′ transcript processing
44 in yeast (Singh and Hampsey 2007; O'Brien and Ansari 2022; O'Brien and Ansari 2023),
45 as well as in transcription termination in mammalian cells (Santana et al. 2022).
46

47 Acute global loss of TFIIB broadly represses gene expression, confirming its central role
48 in cellular transcription (Santana et al. 2022). However, several observations suggest
49 that it may be a point of control during stress. For example, its abundance fluctuates
50 during differentiation (Shiraishi et al. 2009) and retinal damage (Sang et al. 2013), it is
51 depleted during murine gammaherpesvirus infection as mentioned above (Hartenian et
52 al. 2020), and it is relocalized to the cytoplasm by Thogoto virus to alter immune gene
53 expression (Haas et al. 2018). TFIIB is further subject to regulation through protein
54 modifications including phosphorylation (Wang et al. 2010; Shandilya et al. 2012),
55 acetylation (Choi et al. 2003), and ubiquitination (Watanabe et al. 2020).
56
57 Here, we reveal that a variety of stresses converge on TFIIB, regulating its abundance
58 via a caspase-mediated cleavage event in B and T lymphocytes. Cleavage occurs at a
59 conserved residue located between the two cyclin folds of TFIIB that contact promoter
60 DNA. We used exogenous expression in B cells and endogenous base editing in T cells
61 to show that an uncleavable allele of TFIIB causes selective upregulation of short,
62 stress-response genes during apoptosis. Even though many TFIIB-sensitive genes are
63 not constitutively expressed in unstressed cells, we find their promoters are nonetheless
64 pre-loaded with TFIIB and RNAP II to enable rapid induction and subsequent
65 transcriptional regulation. Cells that cannot cleave TFIIB to dampen expression of these
66 genes aberrantly proliferate during chemical stress and upregulate transcription from an
67 oncogenic human herpesvirus. Together, our data suggest that TFIIB cleavage tempers
68 transcription at stress response and mitogenic genes in apoptotic lymphocytes,
69 functioning as a stress-activated mechanism to drive transcriptional repression.

70

71 ## Results

72

73 **Cellular stress induces caspase cleavage of TFIIB at residue D207**

74

75 We first evaluated whether TFIIB loss is a general feature of cellular stress. We focused
76 on immune cells, as B and T lymphocytes are highly sensitive to stress (Muralidharan
77 and Mandrekar 2013) and B cells are a primary infection target of several oncogenic
78 gammaherpesviruses. TFIIB protein levels were assessed in a B cell lymphoma line
79 (TRExRTA BCBL-1, henceforth referred to as BCBL-1) that latently harbors the human
80 herpesvirus Kaposi's sarcoma-associated herpesvirus (KSHV) (Nakamura et al. 2003).
81 Cells were subjected to several stressors, including the DNA damage agent etoposide,
82 the translation inhibitor cycloheximide, or lytic reactivation of KSHV via doxycycline
83 (dox)-induced expression of the master viral lytic activator, RTA. Western blotting
84 revealed that all three treatments reduced endogenous TFIIB protein, suggesting that it
85 is commonly targeted during stress **(Fig. 1A)**.

86

87 The reduction of TFIIB under stress conditions was associated with the appearance of
88 smaller molecular weight bands in the ~20 kD range. A stably introduced version of
89 TFIIB fused to a 2x C-terminal strep tag in BCBL-1 cells was similarly cleaved and
90 yielded a ~14 kD strep-tagged product, suggesting that TFIIB proteolysis occurs closer
91 to the C-terminus of the protein (**Fig. 1A**). TFIIB phosphorylation is not linked to the
92 appearance of these smaller species, as phosphomimetic S65E and

93 unphosphorylatable S65A TFIIB displayed the same degradation pattern as wild-type
94 (WT) TFIIB (Shandilya et al. 2012) **(Supplemental Fig. S1A)**.
95
96 Stress-induced proteolytic cleavage is a hallmark of caspase activity. To test the
97 involvement of caspases in TFIIB cleavage, we treated with the apoptosis-inducing
98 TRAIL ligand, which causes a shift from inactive, executioner procaspase-3 to its
99 cleaved, active form. TRAIL causes the same appearance of smaller TFIIB bands as
100 other stressors (**Fig. 1B**). This was also observed in Jurkat T cells, a model system for
101 studying apoptosis (**Fig. 1C)**. We identified a putative caspase-3 cleavage site after
102 TFIIB aspartic acid residue 207 using CaspSites, a repository for caspase substrates
103 (Wang and Julien 2023). Mutation of this site to alanine (D207A) in strep-tagged TFIIB
104 rendered the protein resistant to cleavage, confirming this as the primary cleavage site
105 **(Fig. 1D)**. Both the pan-caspase inhibitor Z-VAD-OMe-FMK and the caspase-3/7
106 inhibitor Z-DEVD-FMK impaired TFIIB-2xStrep cleavage during TRAIL-induced
107 apoptosis relative to the Z-FA-FMK negative control (**Fig. 1E**). Caspase-3 and caspase-
108 7 share overlapping substrate motifs, and we thus assessed their relative contribution to
109 TFIIB cleavage (McStay et al. 2008; Julien and Wells 2017). Individual siRNA
110 knockdown of caspase-3 or caspase-7 extended the half-life of full-length TFIIB, with a
111 more pronounced effect observed for caspase-3 and the strongest effect upon co-
112 depletion of both caspases (**Fig. 1F**). Thus, TFIIB cleavage by caspases-3 and 7 at
113 D207 decreases its protein levels during a variety of cellular stresses.
114

115 **TFIIB cleavage controls the expression of stress response pathway elements in**
116 **lymphocytes**
117
118 Sequences surrounding the TFIIB caspase cleavage site are highly conserved across
119 metazoans, and D207 is maintained in fruit flies through humans, though not yeast,
120 hydra, or nematodes (**Fig. 2A**). D207 is in a short, unstructured region bridging the two
121 positively charged cyclin folds of TFIIB that contact promoter DNA (**Fig. 2B,**
122 **Supplemental Fig. S2A**). Thus, caspase cleavage at this site could destabilize TFIIB
123 promoter binding and pre-initiation complex (PIC) formation, leading to repressed
124 transcription.
125
126 To determine if TFIIB D207 cleavage regulates gene expression during pro-apoptotic
127 stress in lymphocytes, we tested the effects of both D207A overexpression in B cells
128 and D207G editing at the endogenous TFIIB locus in T cells. We first generated BCBL-1
129 cells stably expressing strep-tagged WT or uncleavable D207A TFIIB. These cells were
130 mock-treated or treated with TRAIL to induce apoptosis, a condition in which mRNA
131 synthesis is broadly decreased **(Supplemental Fig. S2B)** (Duncan-Lewis et al. 2021),
132 and then subjected to RNA-seq. Endogenous TFIIB was still present in these cells, and
133 thus, this approach should preferentially identify genes that are highly sensitive to TFIIB
134 levels. We performed an exon-intron split analysis (Gaidatzis et al. 2015) to quantify
135 differential expression of nascent transcripts (**Fig. 2C**), which identified 61 upregulated
136 and 2 downregulated genes specific to TRAIL treatment in D207A-expressing cells.
137 Upregulated genes were associated with stress response pathways like TNF-α signaling

138 via NF-κB, UV response, and mTORC1 (**Fig. 2D**). Several of these genes were
139 immediate early/delayed early genes with roles in modulating cell proliferation and
140 apoptosis (e.g., *MYC*, *FOSB, ZFP36*) (Tullai et al. 2007). Analysis of the bulk RNA
141 levels similarly yielded a restricted set of 16 genes upregulated by D207A upon TRAIL
142 treatment, several of which have reported oncogenic or pro-survival roles, including
143 *BCL2* **(Supplemental Fig. S2C**).
144
145 Since BCBL-1 cells are infected with KSHV, we were also able to assess the impact of
146 D207A expression on viral transcription. As a nuclear replicating dsDNA virus, KSHV is
147 dependent on host transcription machinery for viral gene expression. In line with this,
148 the expression of nearly all KSHV genes was modestly increased in lytically reactivated
149 BCBL-1 cells containing the uncleavable version of TFIIB (**Fig. 2E**). These data suggest
150 that host targeting of TFIIB not only regulates lymphocyte responses but can also act in
151 an anti-viral manner during viral replication.
152
153 To extend the above results to T cells in a more native context, we base edited cells
154 (Gaudelli et al. 2017) to introduce a D207G mutation into endogenous TFIIB in Jurkat
155 cells. Two different guides were used (D207G-#1 and D207G-#2); a guide targeting the
156 AAVS1 safe locus served as a control (Lombardo et al. 2011; Li et al. 2019). All guides
157 yielded efficient ($\geq$ 85%) editing with minimal bystander effects, and the D207G
158 mutation was stably maintained (**Supplemental Fig. S3A-D**). Clonal lines with pristine
159 edits were also derived from each guide, although we primarily focused on the pooled
160 lines as clones are known to exhibit variation in gene expression due to drift (Meir et al.

161 2020). The D207G mutation substantially reduced cleavage of TFIIB in pooled
162 populations and abolished cleavage in clonal lines treated with TRAIL relative to control
163 **(Fig. 3A, Supplemental Fig. S4A).**
164
165 To rigorously quantify changes to both bulk and nascent RNA, each of the edited lines
166 and matched controls were mock- or TRAIL-treated and subjected to SLAM-seq (thiol
167 (SH)-Linked Alkylation for the Metabolic Sequencing of RNA) **(Fig. 3B)** (Jürges et al.
168 2018). In line with the BCBL-1 data, the primary phenotype of TRAIL-treated D207G
169 Jurkat cells was significantly increased gene expression of a select group of genes,
170 despite global transcriptional repression (**Supplemental Fig. S5A-B)**. This observation
171 was consistent between guide RNAs **(Fig. 3C-D** for D207G-#1, **Supplemental Fig.**
172 **S5C-D** for D207G-#2**)**. We observed nearly complete overlap in the set of significantly
173 upregulated genes (bulk RNA) from both edited pools **(Fig. 3E)**.
174
175 Enrichment analysis of this set of genes strikingly echoed that of D207A-expressing
176 BCBL-1 cells and was reproduced in sequencing from D207G clonal lines (**Fig. 3F**,
177 **Supplemental Fig. S4B-E)**. Shared pathway associations included TNF-α signaling via
178 NF-κB and inflammatory responses, aligning with lymphocytes' role as professional
179 immune cells. Although there was stochasticity in the individual genes upregulated by
180 uncleavable TFIIB across sequencing sets, we nonetheless observed high coherence in
181 their attributes. As in BCBL-1 cells, genes involved in immunity, cell proliferation, and
182 stress were prevalent, including immediate and delayed early genes such as *IER5L*,
183 *GFPT2, JUNB, SERPINE1, EGR4, ZFP36,* and others (for full gene lists, see

184 **Supplemental Table S1**). Some other stimulus-responsive genes were also
185 upregulated in multiple analyses, including *FN1, IRF7,* and *SOCS* genes. Notably, the
186 upregulated genes in D207G Jurkats and in the D207A-overexpressing BCBL-1 cells
187 were significantly shorter than all genes and their downregulated counterparts,
188 indicating that TFIIB stabilization disproportionally upregulates short transcripts (**Fig.**
189 **3G, Supplemental Fig. S2D)**. Such genes tend to be stimulus-responsive and are often
190 immune-related and/or proto-oncogenic (Tullai et al. 2007; Lopes et al. 2021).
191
192 **TFIIB cleavage dampens expression of stress-induced genes with pre-assembled**
193 **RNAP II PICs**
194
195 We were intrigued by the observation that TFIIB cleavage controls many stress-
196 responsive genes. In general, such loci are not constitutively expressed at high levels
197 but rather are rapidly induced following perturbation and need to be efficiently
198 downregulated as the cell resolves the stress or undergoes apoptosis (Bahrami and
199 Drabløs 2016). Holistically, genes upregulated in D207G-edited Jurkat cells indeed
200 exhibit lower or undetectable expression under basal conditions and are upregulated
201 after stimulation with TRAIL **(Fig. 4A-B, Supplemental Fig. S6A)**. We wondered if this
202 transcription induction required *de novo* PIC assembly or whether their promoters are
203 pre-loaded with TFIIB and RNAP II.
204
205 To measure TFIIB and RNAP II occupancy at TFIIB cleavage-sensitive genes, we
206 performed chromatin immunoprecipitation and sequencing (ChIP-seq) using antibodies

207 against the N-terminus of the RNAP II catalytic subunit RPB1 or against V5 in Jurkat
208 cells stably expressing V5-tagged TFIIB (TFIIB-V5). We used an siRNA-resistant TFIIB-
209 V5 under an inducible promoter, such that doxycycline induction with siRNA-mediated
210 depletion of endogenous TFIIB yielded tagged TFIIB protein expression at near-
211 endogenous levels (**Supplemental Fig. S6B-C**). As expected, there was broad
212 promoter occupancy of RPB1 and TFIIB in mock cells and a strong reduction in
213 occupancy of both upon TRAIL treatment, which corresponded well with a general
214 suppression of the transcriptome by RNA-seq (**Supplemental Fig. S6D-F**). The cleaved
215 TFIIB-V5 fragment did not appear to occupy DNA independently since the correlation of
216 RPB1 and V5 binding during TRAIL treatment did not differ substantially from mock, and
217 there were no V5-enriched loci in the absence of RPB1 binding (**Supplemental Fig.**
218 **S6G).**
219
220 Metagene profiles revealed that TFIIB D207G-sensitive genes contained both RNAP II
221 and TFIIB in unstressed (mock) cells (**Fig. 4C-D, Supplemental Fig. S7A-B**), even
222 though most genes were not strongly expressed under these conditions (**Fig. 4A,**
223 **Supplemental Fig. S6A**). However, upon TRAIL treatment — when their gene
224 expression was induced — TFIIB-V5 levels were diminished (**Fig. 4D**). This suggests
225 that rather than *de novo* PIC recruitment at these loci, cells maintain ongoing RNAP II
226 initiation and pausing for a swift transcriptional response upon perturbation, a
227 characteristic of rapid response genes (Tullai et al. 2007). The observation that the
228 TFIIB D207G mutation leads to enhanced levels of transcriptional induction indicates

229 that TFIIB cleavage at these loci dampens their transcription, perhaps to prevent an
230 over-exuberant response.
231
232 Some stress response genes are regulated by Negative Elongation Factor (NELF)-
233 mediated RNAP II promoter pausing, which prevents transcriptional elongation until
234 relieved during stimulation (Amir-Zilberstein et al. 2007; Gilchrist et al. 2008; Bahrami
235 and Drabløs 2016). Consistent with this model, we found that TFIIB cleavage-sensitive
236 genes in lymphocytes were significantly enriched for targets of NELFE **(Fig. 4E)**.
237 Analysis of published NELFE ChIP-seq in K562 cells (ENCODE 2012) confirmed a peak
238 of NELFE occupancy near transcription start sites of these loci **(Supplemental Fig.**
239 **S7C)**.
240
241 These genes were also enriched for associations with other transcription factors,
242 including KLF4 **(Fig. 4E)**, a known regulator of several pathways that coincide with our
243 recurrent MSigDB enrichments, including TGF-β and NF-κB (Ghaleb and Yang 2017).
244 Discriminative MEME analysis of regions upstream of these loci showed enrichment for
245 a GC-rich KLF and SP transcription factor family binding motif **(Supplemental Fig.**
246 **S7D)**. We verified with available MCF-7 ChIP data that promoter regions of D207G-
247 induced genes exhibit occupancy of both KLF4 and SP1 **(Supplemental Fig. S7C)**
248 (ENCODE 2012). Like KLF4, SP1 is a modulator of NF-κB-driven gene expression and
249 of immediate response genes (Hirano et al. 1998; Fowler et al. 2011). Collectively, these
250 data highlight how stress response genes that are highly sensitive to TFIIB cleavage

251 may be regulated by specific transcription factor interactions with RNAP II machinery
252 constitutively present at their promoters.
253
254 **Failure to cleave TFIIB causes aberrant proliferation of cells treated with**
255 **etoposide and antimycin A**
256
257 Since TFIIB cleavage during stress dampens the transcription of some mitogenic and
258 pro-survival stress response genes, we hypothesized that failure to cleave TFIIB may
259 cause aberrant cellular proliferation. We therefore performed a cell growth assay in
260 which GFP-labelled control and mCherry-labelled D207G Jurkat cell pools were
261 competed against each other in the presence of stress-inducing agents, including drugs
262 with chemotherapeutic, anti-inflammatory, and neurological effects (**Fig. 5A**). The ratio
263 of mCherry to GFP was calculated as a proxy for D207G cell fitness.
264
265 Among the panel of chemical stressors tested, two candidates significantly altered the
266 D207G:control ratio **(Supplemental Fig. S8A-B)** — the topoisomerase inhibitor
267 etoposide, which is a chemotherapeutic agent used to treat various cancers, including
268 those caused by KSHV, and the mitochondrial stressor antimycin A. The D207G cells
269 outgrew the control cells in both cases and in a dose-dependent manner **(Fig. 5B,**
270 **Supplemental Fig. S8C-D)**. This was not due to accelerated basal proliferation, as the
271 D207G:control ratio in untreated and DMSO-treated populations did not increase over
272 time. Thus, the inability to cleave TFIIB during stress can dispose cells to an abnormal
273 state of proliferation.

274

275 ## Discussion

276

277 Here, we uncover a mechanism by which cells dynamically alter protein abundance of
278 the basal RNAP II general transcription factor TFIIB during a variety of stresses,
279 including TRAIL treatment, DNA damage, translational stress, and KSHV lytic
280 reactivation. Executioner caspases-3/7 cleave TFIIB at a highly conserved site located
281 between its two cyclin folds that engage promoter DNA, which may impair its ability to
282 form and maintain stable pre-initiation complexes. This tunes the expression of a select
283 set of stress-responsive loci at which TFIIB-containing PICs are pre-assembled but
284 largely quiescent until stimulated. Stressed cells unable to cleave TFIIB exhibit
285 excessive transcription of these genes, a number of which are associated with pro-
286 survival and mitogenic signaling. Functionally, we demonstrate that this can result in
287 increased KSHV lytic gene expression and aberrant cellular proliferation **(Fig. 5C)**.

288

289 **Stress selectively reshapes transcription by targeting RNAP II protein machinery**

290

291 Rapid responses to environmental stimuli are essential for viability. Repression of bulk
292 transcription may play a key role in shifting resources to activate stress response or
293 antiviral genes, as well as potentiate cellular shutdown when cell death is triggered.
294 Several mechanisms exist to post-translationally regulate RNAP II, including ubiquitin-
295 mediated degradation of the RNAP II catalytic subunit RPB1 during genotoxic stress
296 (Wilson et al. 2013; Caron et al. 2019; Tufegdžić Vidaković et al. 2020). This promotes

297 temporary transcriptional shutdown of short, pro-growth and oncogenic transcripts
298 (Tullai et al. 2007; Tufegdžić Vidaković et al. 2020).
299
300 Analogously, caspase-mediated decay of TFIIB during cellular stress suppresses
301 improper activation of a subset of genes, many of which are short and have reported
302 oncogenic activity. Despite the broad requirement for TFIIB at cellular promoters
303 (Santana et al. 2022), we found that a restricted number of transcripts are highly
304 sensitive to TFIIB cleavage. The ability of a core component of the transcriptional
305 machinery to selectively impact specific genes has also been observed in the broader
306 scope of the RNAP II holoenzyme; for example, degron-tagging and depletion of RNAP
307 II complex subunits revealed considerable heterogeneity in transcriptional responses (Li
308 et al. 2022). Hence, while the integrity of basal RNAP II machinery is important for
309 cellular homeostasis, there are surprisingly specific regulatory effects from modulating
310 its individual components.
311
312 **TFIIB cleavage sensitivity and gene expression kinetics**
313
314 Our data indicate that genes sensitive to TFIIB cleavage in lymphocytes are
315 predominantly stress-induced, including immediate early response genes and those
316 associated with pro-survival and inflammatory responses. Basal occupancy of RNAP II
317 and TFIIB at many of these loci in unperturbed cells points to their being readied for
318 rapid activation upon stimulation but restrained until then by factors like NELFE that
319 prevent RNAP II elongation. Their expression may also be coordinated by transcription

320 factors such as KLF4 and SP1, which appear to bind the promoter regions of TFIIB-
321 responsive genes and have been linked to many of the same pathways. A previous
322 study of TFIIB knockdown in HeLa cells found that TFIIB-sensitive genes require *de*
323 *novo* RNAP II recruitment (Haas et al. 2018). Although we observe basal RNAP II
324 occupancy at TFIIB-sensitive genes in T cells, this does not preclude additional RNAP II
325 recruitment to TFIIB-sensitive promoters. Upon stimulation, we hypothesize that the pre-
326 assembled TFIIB-containing PICs initiate multiple rounds of transcription of stress
327 response genes. However, as caspase activation decreases TFIIB, this eventually leads
328 to downregulation of these promoters and perhaps shifts gene expression towards cell
329 death. In this way, TFIIB could serve as a rheostat, tuning transcription appropriately
330 based on its protein levels and the cell stress context.
331
332 The temporality of TFIIB cleavage may influence shifts in gene expression. Intriguingly,
333 the TSVD caspase-3/7 recognition motif within TFIIB does not adhere to the optimal
334 DEVD recognition motif, nor does it contain the canonical negatively charged residue in
335 the P4 position (Julien and Wells 2017). The non-canonical TS residues in the
336 respective P4 and P3 locations may attenuate caspase recognition efficiency (Julien
337 and Wells 2017) and potentially delay cleavage of TFIIB relative to other substrates.
338 Cells with less potent cell death pathways may consequently retain greater TFIIB
339 abundance. Conversely, not all caspase activity results in apoptosis (Nakajima and
340 Kuranaga 2017), and thus, caspase-mediated regulation of TFIIB may also influence
341 processes unrelated to cell death.
342

343 **Physiological context of TFIIB regulation**

344

345 B and T lymphocytes exhibit high rates of turnover (Young et al. 1995) and are strictly
346 controlled by cell death at various stages, including during maturation and in the post-
347 immune response “contraction” phase (Zhang et al. 2005; Shah et al. 2021). These cells
348 exist under a fine balance of cell death and survival pathways (Thome and Tschopp
349 2001; Sen 2006), the dysregulation of which can lead to lymphoproliferative disorders
350 (Justiz Vaillant and Stang 2025). In this regard, our finding that TFIIB(D207G)-edited
351 cells have a competitive growth advantage during mitochondrial stress and DNA
352 damage underscores the physiological importance of this mechanism of TFIIB
353 regulation.

354

355 We also found that viral gene expression in KSHV-reactivated B cells was boosted in
356 the presence of uncleavable TFIIB. Control of TFIIB, and more broadly RNAPII, is an
357 important component of virus-host interactions (O'Brien and Ansari 2021; Gulyas and
358 Glaunsinger 2022). RNA viruses that do not use cellular RNAPII for gene transcription
359 can selectively cripple host gene expression by targeting core general transcription
360 factors like TFIIB, thereby limiting antiviral gene expression (Vogt et al. 2008; Haas et
361 al. 2018). However, nuclear replicating DNA viruses must hijack cellular transcriptional
362 machinery for viral gene expression. Caspase regulation of TFIIB may therefore also be
363 an antiviral response geared towards restricting viral access to functional transcriptional
364 machinery while maintaining sufficient levels to activate anti-viral genes. Future

365 research on the biophysical and temporal control of this process should yield key
366 insights into how cells and viruses tune gene expression through modulation of TFIIB.
367
368
369 ## Materials and Methods
370
371 Methods for supplemental data are found in **Supplemental Materials and Methods**.
372
373 **Cloning**
374
375 The TFIIB sequence (synthesized by Twist Bioscience) for cloned constructs was
376 modified to preserve the amino acid sequence but be resistant to Dharmacon OnTarget
377 and Accell human *GTF2B* siRNAs. For strep-tagged constructs, TFIIB was Infusion
378 (Takara Bio) cloned into XhoI site of pcDNA4/TO-2xStrep (pCDNA4/TO Invitrogen
379 vector modified to include a C-terminal 2xStrep tag). TFIIB-2xStrep was Infusion cloned
380 into the Sfi1 site of a sleeping beauty plasmid pSBbi-GP (Addgene #60511, gift from
381 Eric Kowarz) derivative lacking EGFP to make the TFIIB-2xStrep expression vector
382 (Addgene #213919). Derivative point mutant plasmids D207A, S65A, and S65E
383 (Addgene # pending) were made by inverse PCR as described previously (Silva et al.
384 2023). The siRNA resistant 6xHis-TFIIB-V5 construct was synthesized by Twist,
385 amplified, and InFusion subcloned with a PCR-amplified sleeping beauty plasmid
386 pSBtet-BB backbone (Addgene #60505, gift from Eric Kowarz) (Addgene # pending).
387 Sleeping beauty vectors and the sleeping beauty transposase plasmid were provided by

388 Nicholas Ingolia (UC Berkeley); the sleeping beauty system was described previously
389 (Kowarz et al. 2015).
390
391 All plasmids were validated by full-plasmid sequencing and deposited on Addgene.
392 Primer and DNA sequences are available in **Supplemental Table S2**.
393
394 **Cell line generation, maintenance, and reactivation**
395
396 All cell lines were maintained at 37°C and 5% CO_2 in a humidity-controlled incubator,
397 and cell density was kept at 0.5- 2 × 10^6 cells/mL. TRExRTA BCBL-1 cells (generously
398 provided by the lab of Jae Jung) (Nakamura et al. 2003) were maintained in RPMI 1640
399 media (Gibco) supplemented with 10% Tet-free fetal bovine serum (FBS; via UC
400 Berkeley Cell Culture Facility), 1X GlutaMAX (Gibco), and 10 μg/mL hygromycin B
401 (Invitrogen). Unless otherwise noted, cell concentration was ~1 × 10^6 cells/mL when
402 reactivated with 1 μg/mL doxycycline or drug-treated. Jurkat cells (obtained from the UC
403 Berkeley Cell Culture facility) were maintained in RPMI 1640 media (Gibco) with 1X
404 GlutaMAX (Gibco), 10 % Tet-free FBS (via UC Berkeley Cell Culture Facility), 1mM
405 sodium pyruvate, and 1X Pen-Strep (Gicbo).
406
407 BCBL-1 derivatives were generated by nucleofection with the Neon Transfection
408 System (Invitrogen) according to the manufacturer's instructions with the following
409 parameters: 5 × 10^6 low-passage cells were pulsed (1350 V, 1 × 40 ms pulse-length)
410 with 2 μg DNA in a 100 μL tip. The TFIIB-2xStrep vector and point mutant derivatives
were

411 delivered with a 1:20 mass ratio of transposase to delivery vector. Cells were selected
412 with 1 μg/mL puromycin 24 h post-nucleofection. 6xHis-TFIIB-V5 expressing Jurkat
413 cells were generated identically but with 2.5 μg DNA (1700 V, 1 × 20 ms pulse-length)
414 and 10 μg/mL blasticidin HCl (Gibco) selection.
415
416 **Jurkat base-editing and labeling**
417
418 Cells were base edited by nucleofecting (Neon Transfection System per manufacturer's
419 instructions; 1700 V, 1 × 20 ms pulse-length, 10 μL tip) 1×10^6 low passage Jurkat cells
420 with 1.63 μg A•G base editor RNA and 1 μg sgRNA (IDT) containing target sequences
421 (**Supplemental Table S2**) predicted by the UCSC Genome Browser (Perez et al. 2025).
422 The AAVS1 safe sequence was previously published (Li et al. 2019). The *in vitro* ABE8e
423 base editor RNA from Addgene #138489 (gift of David Liu) was generously provided by
424 Dr. Fyodor Urnov (UC Berkeley).
425
426 mCherry (pLVX-mCherry-P2A-Blasticidin) and GFP **(**pLVX-GFP-P2A-Blasticidin)
427 (Haakonsen et al. 2024) labelling plasmids were generously provided by Michael Rapé
428 (UC Berkeley). Labelling of base-edited pooled populations was performed via 2nd
429 generation lentiviral transduction: 1×10^6 Lenti-X 293T cells (Clonetech/Takara via the
430 UC Berkeley Tissue Culture Facility) maintained in DMEM (Gibco) with 10% FBS were
431 transfected (manufacturer's protocol) using Mirus *Trans*IT-293 Transfection Reagent
432 with 250 ng pCMV-VSV-G (Addgene #8454, gift of Bob Weinberg), 1250 ng psPAX2
433 (Addgene #12260; gift of Didier Trono), and 1250 ng lentivector. Lentivirus was

434 harvested at 48 h, 0.45 μm filtered, and 3 mL of viral product was mixed with 5 × 10^6
435 base edited Jurkat cells in 2 mL of media (D207G guide populations received mCherry;
436 AAVS1 control received GFP), and 10 μg/mL polybrene (Sigma). Cells were spinfected
437 at 800 × g for 2 h at 32ºC, resuspended in 5 mL fresh media, recovered for 48 h, and
438 selected with 5 μg/mL blasticidin HCl.
439
440 **siRNA knockdowns**
441
442 After 24h of doxycycline-induction (2.5 μg/mL) of siRNA-resistant 6xHis-TFIIB-V5 in
443 Jurkat cells, endogenous protein was knocked down by siRNA. 3 × 10^6 Jurkat cells
444 were prepared in 100 μL of resuspension buffer T (Invitrogen) and 3 μM of the following
445 Dharmacon siRNAs: On-Target Plus Non-targeting control pool and Accell Non-targeting
446 control pool for non-targeting control cells, or On-Target Plus human *GTF2B* siRNA
447 SmartPool and Accell human *GTF2B* siRNA SmartPool for TFIIB knockdown cells. Cells
448 were nucleofected (1700 V, 1 × 20 ms pulse-length) with the Neon Transfection System
449 (Invitrogen) according to the manufacturer's instructions. siRNA treatments for ChIP-
450 sequencing were performed identically on 10 × 10^6 Jurkat cells with 10 μM each of On-
451 Target Plus human *GTF2B* siRNA SmartPool and Accell human *GTF2B* siRNA
452 SmartPool.
453
454 Caspase-3/7 knockdowns were performed with the following modifications: 3 × 10^6
455 BCBL-1 cells were nucleofected (1350 V, 1 × 40 ms pulse-length) in 3 μM of either
456 Dharmacon human *Casp3* and/or *Casp7* Accell SmartPool siRNA and 3 uM Dharmacon

457 human OnTarget *Casp3* and/or *Casp7* SmartPool. Non-targeting Accell and OnTarget
458 siRNA (siNTC) was used as a control.
459
460 **Western blotting**
461
462 Cells were lysed in 1% SDS RIPA buffer (1% SDS, 1% NP40, 150 mM NaCl, 50 mM
463 Tris-HCl pH 8, 0.5% sodium deoxycholate by mass) with Halt Protease and
464 Phosphatase Inhibitor Cocktail (Thermo Scientific), followed by sonication (1 min, 100
465 A, 3 s on/17 s off), 1% Benzonase (Millipore) treatment, and centrifugation (21,000 x g,
466 10 min, 4°C). Diluted samples were quantified by Pierce 660 assay with 0.8% Triton-X.
467 10-30 μg lysate was denatured in Laemmli Buffer (Bio-Rad), resolved by SDS-Page and
468 transferred to PVDF membrane with a Trans-Blot Turbo apparatus (Bio-Rad, Mixed
469 Molecular Weight protocol). Western blotting was performed with Tris-buffered saline
470 and 0.2% Tween-20 and the following primary and secondary antibodies: TFIIB (clone
471 2F6A3H4, Cell Signaling- 4169, 1:1000), GAPDH (anti-mouse, clone 6C5,
472 Thermofisher-AM4300, 1:5000 or anti-rabbit, clone 14C10, Cell Signaling-2118,
473 1:1000), Vinculin (Abcam- ab91459, 1:1000), Caspase-3 (Cell Signaling-9662, 1:1000),
474 Caspase-7 (Cell Signaling-9492, 1:1000), V5 (clone D3H8Q, Cell Signaling-13202),
475 Goat Anti-Mouse IgG(H+L) or Goat Anti-Rabbit IgG(H+L) Human ads-HRP (Southern
476 Biotech, 1:5000), Strep-Tag II Antibody HRP Conjugate (Sigma Aldrich-71591-3,
477 1:2000). Blots were developed with Clarity Western ECL Substrate (Bio-Rad) or
478 Radiance Plus Femtogram-sensitivity HRP Substrate (Azure Biosystems). Blots were
479 imaged on a Chemidoc MP imager (Bio-Rad) and prepared for publication using Bio-

480 Rad Image Lab v. 6.0.1 with the autoscale feature to maintain consistency unless
481 otherwise noted. Blots shown are representative of a minimum of 3 biological replicates
482 at the same conditions and/or timepoints.
483
484 **RNA-sequencing**
485
486 RNA-seq experiments were conducted in triplicate as follows with the noted
487 specifications. Cells were washed and pelleted, then total RNA was collected in 1 mL
488 TRIzol (Invitrogen) and isolated by 1 × 200 uL chloroform extraction as outlined
489 previously (Toni et al. 2018), including precipitation in 500 uL isopropanol with 1%
490 glycogen and 10% 3 M sodium acetate. RNA concentration was quantified by Qubit 3
491 Fluorometer with High Sensitivity RNA Kit (Invitrogen). Prior to library prep, ERCC RNA
492 Spike-in mix (Invitrogen) was added to all input samples per the manufacturer's
493 instructions. TFIIB-2xStrep/TFIIB(D207A)-2xStrep libraries were prepped by the KAPA
494 RNA Hyperprep Kit with RiboErase (Roche) using 1,000 ng input RNA, with
495 fragmentation at 94°C for 6 min, ligation with KAPA Unique Dual-Indexed adaptors
496 (Roche), and amplification for 7 cycles. Library quality was confirmed on an AATI (now
497 Agilent) Fragment Analyzer. Library molarity was measured via quantitative PCR with
498 the KAPA Library Quantification Kit (Roche KK4824) on a BioRad CFX Connect thermal
499 cycler. Libraries were then pooled by molarity and sequenced, targeting at least 25M
500 reads per sample. TFIIB-2xStrep/TFIIB(D207A)-2xStrep libraries were sequenced on an
501 Illumina NovaSeq X 10B with 150 bp paired-end reads. Fastq files were generated and

502 demultiplexed using Illumina bcl_convert and default settings, on a server running
503 CentOS Linux 7.
504
505 Analysis was modified from the UC Davis Bioinformatics Core RNA-seq workflow.
506 Sequencing quality was assessed with MultiQC, and reads were preprocessed with
507 HTStream v. 1.3.0, including deduplication. Genome indices were prepared using STAR
508 v. 2.7.1a (Dobin et al. 2013). The human GRCh38.p13 genome assembly (ensembl.org)
509 was indexed with Gencode v43 annotations. Due to overlapping transcripts on the
510 KSHV-BAC16 genome, individual exon coordinates were assigned to the parent viral
511 transcript in a custom gene annotation. Preprocessed reads were aligned with STAR,
512 and count files were generated for transcripts. Viral counts were imported to Microsoft
513 Excel and normalized to the sum of ERCC spike-in counts. Replicates were then
514 normalized to their corresponding mock condition and averaged. Any transcript with no
515 reads in some or all replicates and conditions was eliminated from further analysis.
516 Heatmaps were generated using the matplotlib, pandas, and seaborn packages in
517 Spyder v. 5.3.3. Nascent cellular RNA counts were estimated by the eisaR package as
518 described (Gaidatzis et al. 2015). Library size normalization (TMM method) was used
519 since bulk RNA of the same treatment showed minimal variance. Differential gene
520 expression analysis for bulk and nascent RNA was conducted in RStudio v.
521 2024.12.1+563 with the Bioconductor package using edgeR with limma/voom
522 developed and described by Law et al. (Law et al. 2018). Bulk RNA was normalized to
523 ERCC Spike-In and multiple testing was compensated for using the Benjamini-
524 Hochberg correction. Gene annotations are from the BioMart Ensembl Genes 109

525 database. Plots and statistics were generated with R ggplot2 and VennDiagram.
526 Enrichment analyses are from Molecular Signatures Database Hallmark 2020 and
527 Encode and ChEA Consensus TFs from ChIP-X via EnrichR (Liberzon et al. 2011; Chen
528 et al. 2013; Kuleshov et al. 2016; Xie et al. 2021).
529
530 Raw data and counts tables for RNA-seq experiments are available on the GEO
531 database (accession numbers pending).
532
533 *SLAM-sequencing*
534 SLAM-seq was performed as above but with the following modifications. After 3 h
535 treatment of SUPERKILLER TRAIL (250 ng/mL; Enzo) or mock diluent, 300 μM of 4-
536 thiouridine (4sU) or PBS control was added to 3×10^6 cells. Cells were harvested 3 h
537 post-4sU for RNA or western blot. RNA extraction (2 × 200 uL chloroform extraction)
538 and alkylation were performed using the Lexogen SLAM-seq Anabolic Kinetics Kit
539 according to the manufacturer's instructions with 2 μL GlycoBlue (Invitrogen) as a co-
540 precipitant. RNA integrity was checked by TapeStation (Agilent) and quantified using
541 Qubit Broad Range Sensitivity RNA reagents. ERCC RNA Spike-in mix (Invitrogen) was
542 added to inputs per the manufacturer's instructions along with 5 ng of *in vitro*
543 transcribed mixture of both unlabeled and 4sU-labeled spike-ins (synthesized as
544 described previously (Schwalb et al. 2016; Gressel et al. 2019)).
545
546 Inputs for pooled (1000 ng) and clonal (700 ng) line sequencing were alkylated, then
547 samples were DNase-treated and repurified with RNA Clean and Concentrator kits

548 (Zymo). Quality and concentration were reassessed by TapeStation and Qubit (~500 ng
549 final input). Library preparation was performed with fragmentation at 94ºC for 6 minutes.
550 Pooled line samples were ligated with 3 μM adaptor and amplified for 9 PCR cycles;
551 clonal samples were ligated with 1.5 μM and amplified for 10 cycles. Samples were
552 sequenced on a Novaseq X Plus 25B with 150 bp paired-end reads. Incorporation of
553 4sU was validated by visualization on IGV (Robinson et al. 2011). Nascent RNA counts
554 were estimated using GRAND-SLAM with default parameters (Jürges et al. 2018). Total
555 count values were multiplied by the MAP statistic (nascent-to-total ratio) to yield
556 approximate nascent counts; inestimable values were considered 0. Nascent and bulk
557 RNA counts were analyzed using edgeR and limma/voom with ERCC Spike-in
558 normalization from bulk RNA. RNA coverage plots were generated using deepTools
559 (Ramírez et al. 2016) bamCoverage with spike-in normalized --scaleFactor inputs.
560 BigWig files for biological triplicates were averaged with bigwigAverage (--binSize 1)
561 and visualized in IGV.
562
563 **ChIP-sequencing**
564 *Library preparation and sequencing*
565 Jurkat cells expressing 6xHis-TFIIB-V5 were prepared and siRNA-treated as described.
566 After 24 h, 40 × 10^6 cells were dosed with 250 ng/mL SUPERKILLER TRAIL (Enzo) or
567 mock diluent for 4 h. Samples were prepared and DNA sequenced as described
568 previously (Lari et al. 2025) with the following modifications: during immunoprecipitation,
569 10 µg of purified chromatin was incubated with 5 µg rabbit monoclonal anti-RPB1 NTD
570 (clone D8L4Y; Cell Signaling 14958), rabbit polyclonal anti-V5 (Abcam ab15828), or

571 rabbit IgG (Abcam ab37415) overnight. During library preparation, yeast spike-in DNA
572 (Cell Signaling) was added for downstream normalization.
573
574 *Data analysis and visualization*
575 Sequencing quality was assessed with FastQC, and files were trimmed with
576 Trimmomatic v. 0.39 (Bolger et al. 2014). The human (hg38) and yeast (SacCer3)
577 genomes were manually indexed using the bowtie2-build command. Processed
578 sequencing files were aligned to the genomes with bowtie2 v. 2.5.2. Calculated spike-in
579 normalization factors were proportional to the number of spike-in reads per sample and
580 applied to generate BigWig files with bamCoverage (--binSize 10, --smoothLength 30, --
581 extendReads, --centerReads, --normalizeUsing None, and --scaleFactor with the
582 respective spike-in normalized scale factor). Biological duplicate files were averaged
583 with the deepTools bigwigCompare function.
584
585 Matrices for Rpb1 and V5 coverage profiles were made with deepTools computeMatrix
586 scale-regions command on the averaged BigWig files (-S), with --skipZeros, --
587 missingDataAsZero. Bedfiles were obtained from Ensembl BioMart transcript
588 coordinates. ChIP-seq signal was plotted with plotHeatmap as a histogram with 10bp
589 bins, 100 bins/gene. ChIP-seq data are deposited on the GEO database (accession
590 number pending).
591
592 **Competition assays**
593

594 1.5×10^5 cells each of mCherry-labelled D207G pool and GFP-labelled control pool
595 were co-cultured in 1 mL media with the indicated times and drug concentrations
596 (dissolved in DMSO). Population fluorescence was assessed by flow cytometry on a BD
597 Bioscience LSR Fortessa. 10,000 events/sample were collected, and replicates
598 represent independent competitions on separate days. All data were analyzed using
599 FlowJo software (BD Bioscience) with gating for live cells and PE-Texas-Red or FITC
600 positivity. Normalization is indicated in figure legends.
601
602 **Data analysis and data visualization**
603
604 Data quantifications, statistical analyses, and/or visualization for competition assays and
605 enrichment were conducted in GraphPad Prism v. 9-10.10. The Multiple Sequence
606 Alignment (MSA) was generated from TFIIB protein sequences obtained through
607 UniProt (uniprot.org) and analyzed in JalView v. 2.11.4.1 (Waterhouse et al. 2009;
608 Troshin et al. 2011; Troshin et al. 2018) with a human reference and Clustal X
609 coloring/annotation. Protein structures were visualized in UCSF ChimeraX v. 1.9
610 (Pettersen et al. 2021). All schematics were made with BioRender.com (licenses to be
611 added prior to publication).
612
613 ## Competing interests
614 The authors have no competing interests to report.
615
616 ## Acknowledgements

We thank all members of the Glaunsinger and Coscoy labs (UC Berkeley) for their helpful advice and feedback, especially Dr. Chad Stein and Xiaowen Mao. We are also grateful to the following UC Berkeley colleagues: Dr. Fyodor Urnov and Jessica Nguy (Urnov lab) for providing expertise in base editing and A•G base editor RNA, Dr. Michael Rapé and Dr. Michael Heider (Rapé lab) for providing helpful advice and reagents for the drug screen, and Dr. Annan Cook for useful discussions. We thank Dr. Florian Erhard (University of Regensberg) for support using GRAND-SLAM. Finally, we thank the UC Berkeley IGI NGS facility, UCSF ChimeraX (funded by NIH R01-GM12932, Office of Cyber Infrastructure and Computational Biology, NIAID), UC Davis Bioinformatics Core (RRID:SCR_023887) and the UC Berkeley QB3 Genomic Facilities (RRID:SCR_022170) for their services. This research was supported by NIH grants AI122528 and CA136367 to B.G., who is also an investigator of the Howard Hughes Medical Institute.

Author contributions

Conceptualization, L.G. and B.A.G.; methodology, L.G. and B.A.G.; experimentation, L.G., A.L., S.B.S; writing, L.G. and B.A.G.; formal analysis, L.G., A.L, S.B.S., and B.A.G.; project administration, L.G. and B.A.G; supervision and funding acquisition, B.A.G.

640 **References**

641

642 Abernathy E, Gilbertson S, Alla R, Glaunsinger B. 2015. Viral Nucleases Induce an
643 mRNA Degradation-Transcription Feedback Loop in Mammalian Cells. *Cell Host*
644 *Microbe* **18**: 243-253.
645 Amir-Zilberstein L, Ainbinder E, Toube L, Yamaguchi Y, Handa H, Dikstein R. 2007.
646 Differential Regulation of NF-κB by Elongation Factors Is Determined by Core
647 Promoter Type. *Mol Cell Biol* **27**: 5246-5259.
648 Bahrami S, Drabløs F. 2016. Gene regulation in the immediate-early response process.
649 *Adv Biol Regul* **62**: 37-49.
650 Bauer DLV, Tellier M, Martínez-Alonso M, Nojima T, Proudfoot NJ, Murphy S, Fodor E.
651 2018. Influenza Virus Mounts a Two-Pronged Attack on Host RNA Polymerase II
652 Transcription. *Cell Rep* **23**: 2119-2129.e2113.
653 Bolger AM, Lohse M, Usadel B. 2014. Trimmomatic: a flexible trimmer for Illumina
654 sequence data. *Bioinformatics* **30**: 2114-2120.
655 Caron P, Pankotai T, Wiegant WW, Tollenaere MAX, Furst A, Bonhomme C, Helfricht A,
656 De Groot A, Pastink A, Vertegaal ACO et al. 2019. WWP2 ubiquitylates RNA
657 polymerase II for DNA-PK-dependent transcription arrest and repair at DNA
658 breaks. *Genes Dev* **33**: 684-704.
659 Chen EY, Tan CM, Kou Y, Duan Q, Wang Z, Meirelles GV, Clark NR, Ma'Ayan A. 2013.
660 Enrichr: interactive and collaborative HTML5 gene list enrichment analysis tool.
661 *BMC Bioinformatics* **14**: 128.
662 Choi CH, Hiromura M, Usheva A. 2003. Transcription factor IIB acetylates itself to
663 regulate transcription. *Nature* **424**: 965-969.
664 Deng W, Roberts SG. 2007. TFIIB and the regulation of transcription by RNA
665 polymerase II. *Chromosoma* **116**: 417-429.
666 Dobin A, Davis CA, Schlesinger F, Drenkow J, Zaleski C, Jha S, Batut P, Chaisson M,
667 Gingeras TR. 2013. STAR: ultrafast universal RNA-seq aligner. *Bioinformatics*
668 **29**: 15-21.
669 Duncan-Lewis C, Hartenian E, King V, Glaunsinger BA. 2021. Cytoplasmic mRNA
670 decay represses RNA polymerase II transcription during early apoptosis. *Elife* **10**.
671 ENCODE Project Consortium. 2012. An integrated encyclopedia of DNA elements in the
672 human genome. *Nature* **489**: 57-74.
673 Fowler T, Sen R, Ananda. 2011. Regulation of Primary Response Genes. *Mol Cell* **44**:
674 348-360.
675 Gaidatzis D, Burger L, Florescu M, Stadler MB. 2015. Analysis of intronic and exonic
676 reads in RNA-seq data characterizes transcriptional and post-transcriptional
677 regulation. *Nat Biotechnol* **33**: 722-729.
678 Gaudelli NM, Komor AC, Rees HA, Packer MS, Badran AH, Bryson DI, Liu DR. 2017.
679 Programmable base editing of A•T to G•C in genomic DNA without DNA
680 cleavage. *Nature* **551**: 464-471.
681 Ghaleb AM, Yang VW. 2017. Krüppel-like factor 4 (KLF4): What we currently know.
682 *Gene* **611**: 27-37.

683 Gilchrist DA, Nechaev S, Lee C, Ghosh SKB, Collins JB, Li L, Gilmour DS, Adelman K.
684 2008. NELF-mediated stalling of Pol II can enhance gene expression by blocking
685 promoter-proximal nucleosome assembly. *Genes Dev* **22**: 1921-1933.
686 Gressel S, Lidschreiber K, Cramer P. 2019. Transient transcriptome sequencing:
687 experimental protocol to monitor genome-wide RNA synthesis including
688 enhancer transcription. *protocolsio*.
689 Gulyas L, Glaunsinger BA. 2022. RNA polymerase II subunit modulation during viral
690 infection and cellular stress. *Curr Opin Virol* **56**: 101259.
691 Haakonsen DL, Heider M, Ingersoll AJ, Vodehnal K, Witus SR, Uenaka T, Wernig M,
692 Rapé M. 2024. Stress response silencing by an E3 ligase mutated in
693 neurodegeneration. *Nature* **626**: 874-880.
694 Haas DA, Meiler A, Geiger K, Vogt C, Preuss E, Kochs G, Pichlmair A. 2018. Viral
695 targeting of TFIIB impairs de novo polymerase II recruitment and affects antiviral
696 immunity. *PLoS Path* **14**: e1006980.
697 Hartenian E, Gilbertson S, Federspiel JD, Cristea IM, Glaunsinger BA. 2020. RNA
698 decay during gammaherpesvirus infection reduces RNA polymerase II
699 occupancy of host promoters but spares viral promoters. *PLoS Pathog* **16**:
700 e1008269.
701 Hirano F, Tanaka H, Hirano Y, Hiramoto M, Handa H, Makino I, Scheidereit C. 1998.
702 Functional Interference of Sp1 and NF-κB through the Same DNA Binding Site.
703 *Mol Cell Biol* **18**: 1266-1274.
704 Julien O, Wells JA. 2017. Caspases and their substrates. *Cell Death Differ* **24**: 1380-
705 1389.
706 Jürges C, Dölken L, Erhard F. 2018. Dissecting newly transcribed and old RNA using
707 GRAND-SLAM. *Bioinformatics* **34**: i218-i226.
708 Justiz Vaillant AA, Stang CM. 2025. Lymphoproliferative Disorders. in *StatPearls*.
709 StatPearls Publishing, Treasure Island (FL).
710 Kostrewa D, Zeller ME, Armache K-J, Seizl M, Leike K, Thomm M, Cramer P. 2009.
711 RNA polymerase II–TFIIB structure and mechanism of transcription initiation.
712 *Nature* **462**: 323-330.
713 Kowarz E, Löscher D, Marschalek R. 2015. Optimized Sleeping Beauty transposons
714 rapidly generate stable transgenic cell lines. *Biotechnology Journal* **10**: 647-653.
715 Kuleshov MV, Jones MR, Rouillard AD, Fernandez NF, Duan Q, Wang Z, Koplev S,
716 Jenkins SL, Jagodnik KM, Lachmann A et al. 2016. Enrichr: a comprehensive
717 gene set enrichment analysis web server 2016 update. *Nucleic Acids Res* **44**:
718 W90-W97.
719 Lari A, Shah SB, Mao X, Sanghrajka P, Karijolich J, Lareau LF, Glaunsinger BA. 2025.
720 RNA polymerase III transcription-associated polyadenylation promotes the
721 accumulation of noncoding retrotransposons during infection. Cold Spring Harbor
722 Laboratory.
723 Law CW, Alhamdoosh M, Su S, Dong X, Tian L, Smyth GK, Ritchie ME. 2018. RNA-seq
724 analysis is easy as 1-2-3 with limma, Glimma and edgeR. *F1000Research* **5**:
725 1408.
726 Li S, Prasanna X, Salo VT, Vattulainen I, Ikonen E. 2019. An efficient auxin-inducible
727 degron system with low basal degradation in human cells. *Nat Methods* **16**: 866-
728 869.

729 Li Y, Huang J, Zhu J, Bao L, Wang H, Jiang Y, Tian K, Wang R, Zheng H, Duan W et al.
730 2022. Targeted protein degradation reveals RNA Pol II heterogeneity and
731 functional diversity. *Mol Cell* **82**: 3943-3959.e3911.
732 Liberzon A, Subramanian A, Pinchback R, Thorvaldsdóttir H, Tamayo P, Mesirov JP.
733 2011. Molecular signatures database (MSigDB) 3.0. *Bioinformatics* **27**: 1739-
734 1740.
735 Lombardo A, Cesana D, Genovese P, Di Stefano B, Provasi E, Colombo DF, Neri M,
736 Magnani Z, Cantore A, Lo Riso P et al. 2011. Site-specific integration and
737 tailoring of cassette design for sustainable gene transfer. *Nat Methods* **8**: 861-
738 869.
739 Lopes I, Altab G, Raina P, De Magalhães JP. 2021. Gene Size Matters: An Analysis of
740 Gene Length in the Human Genome. *Front Genet* **12**.
741 McStay GP, Salvesen GS, Green DR. 2008. Overlapping cleavage motif selectivity of
742 caspases: implications for analysis of apoptotic pathways. *Cell Death Differ* **15**:
743 322-331.
744 Meir Z, Mukamel Z, Chomsky E, Lifshitz A, Tanay A. 2020. Single-cell analysis of clonal
745 maintenance of transcriptional and epigenetic states in cancer cells. *Nat Genet*
746 **52**: 709-718.
747 Muralidharan S, Mandrekar P. 2013. Cellular stress response and innate immune
748 signaling: integrating pathways in host defense and inflammation. *J Leukoc Biol*
749 **94**: 1167-1184.
750 Nakajima Y-I, Kuranaga E. 2017. Caspase-dependent non-apoptotic processes in
751 development. *Cell Death Differ* **24**: 1422-1430.
752 Nakamura H, Lu M, Gwack Y, Souvlis J, Zeichner SL, Jung JU. 2003. Global Changes
753 in Kaposi's Sarcoma-Associated Virus Gene Expression Patterns following
754 Expression of a Tetracycline-Inducible Rta Transactivator. *J Virol* **77**: 4205-4220.
755 O'Brien MJ, Ansari A. 2021. Critical Involvement of TFIIB in Viral Pathogenesis. *Front*
756 *Mol Biosci* **8**: 669044.
757 -. 2022. Beyond the canonical role of TFIIB in eukaryotic transcription. *Curr Genet* **68**:
758 61-67.
759 -. 2023. Protein interaction network revealed by quantitative proteomic analysis links
760 TFIIB to multiple aspects of the transcription cycle. *Biochim Biophys Acta*
761 *Proteins Proteom* **1872**: 140968.
762 Perez G, Galt, Benet-Pages A, Casper J, Clawson H, Diekhans M, Fischer C, Jairo,
763 Angie, Christopher et al. 2025. The UCSC Genome Browser database: 2025
764 update. *Nucleic Acids Res* **53**: D1243-D1249.
765 Pettersen EF, Goddard TD, Huang CC, Meng EC, Couch GS, Croll TI, Morris JH, Ferrin
766 TE. 2021. UCSF ChimeraX: Structure visualization for researchers, educators,
767 and developers. *Protein Science* **30**: 70-82.
768 Ramírez F, Ryan DP, Grüning B, Bhardwaj V, Kilpert F, Richter AS, Heyne S, Dündar F,
769 Manke T. 2016. deepTools2: a next generation web server for deep-sequencing
770 data analysis. *Nucleic Acids Res* **44**: W160-W165.
771 Robinson JT, Thorvaldsdóttir H, Winckler W, Guttman M, Lander ES, Getz G, Mesirov
772 JP. 2011. Integrative genomics viewer. *Nat Biotechnol* **29**: 24-26.
773 Rosa-Mercado NA, Zimmer JT, Apostolidi M, Rinehart J, Simon MD, Steitz JA. 2021.
774 Hyperosmotic stress alters the RNA polymerase II interactome and induces

775 readthrough transcription despite widespread transcriptional repression. *Mol Cell*
776 **81**: 502-513.e504.
777 Sainsbury S, Niesser J, Cramer P. 2013. Structure and function of the initially
778 transcribing RNA polymerase II–TFIIB complex. *Nature* **493**: 437-440.
779 Sang A, Xu Y, Jin N, Zhou T, Wang J, Zhu J, Chen C, Shi J, Shuai J, Xu G et al. 2013.
780 Involvement of transcription initiation factor IIB in the light-induced death of rat
781 retinal ganglion cells in vivo. *J Mol Histol* **44**: 11-18.
782 Santana JF, Collins GS, Parida M, Luse DS, Price DH. 2022. Differential dependencies
783 of human RNA polymerase II promoters on TBP, TAF1, TFIIB and XPB. *Nucleic*
784 *Acids Res* **50**: 9127-9148.
785 Schwalb B, Michel M, Zacher B, Frühauf K, Demel C, Tresch A, Gagneur J, Cramer P.
786 2016. TT-seq maps the human transient transcriptome. *Science* **352**: 1225-1228.
787 Sen R. 2006. Control of B Lymphocyte Apoptosis by the Transcription Factor NF-κB.
788 *Immunity* **25**: 871-883.
789 Shah K, Al-Haidari A, Sun J, Kazi JU. 2021. T cell receptor (TCR) signaling in health
790 and disease. *Signal Transduct Target Ther* **6**.
791 Shandilya J, Wang Y, Roberts SG. 2012. TFIIB dephosphorylation links transcription
792 inhibition with the p53-dependent DNA damage response. *Proc Natl Acad Sci U*
793 *S A* **109**: 18797-18802.
794 Shiraishi S, Tamamura N, Jogo M, Tanaka Y, Tamura T-A. 2009. Rapid proteasomal
795 degradation of transcription factor IIB in accordance with F9 cell differentiation.
796 *Gene* **436**: 115-120.
797 Silva D, Santos G, Barroca M, Costa D, Collins T. 2023. Inverse PCR for Site-Directed
798 Mutagenesis. pp. 223-238. Springer US.
799 Singh BN, Hampsey M. 2007. A Transcription-Independent Role for TFIIB in Gene
800 Looping. *Mol Cell* **27**: 806-816.
801 Thome M, Tschopp J. 2001. Regulation of lymphocyte proliferation and death by flip.
802 *Nat Rev Immunol* **1**: 50-58.
803 Toni LS, Garcia AM, Jeffrey DA, Jiang X, Stauffer BL, Miyamoto SD, Sucharov CC.
804 2018. Optimization of phenol-chloroform RNA extraction. *MethodsX* **5**: 599-608.
805 Troshin PV, Procter JB, Barton GJ. 2011. Java bioinformatics analysis web services for
806 multiple sequence alignment—JABAWS:MSA. *Bioinformatics* **27**: 2001-2002.
807 Troshin PV, Procter JB, Sherstnev A, Barton DL, Madeira F, Barton GJ. 2018. JABAWS
808 2.2 distributed web services for Bioinformatics: protein disorder, conservation and
809 RNA secondary structure. *Bioinformatics* **34**: 1939-1940.
810 Tufegdžić Vidaković A, Mitter R, Kelly GP, Neumann M, Harreman M, Rodríguez-
811 Martínez M, Herlihy A, Weems JC, Boeing S, Encheva V et al. 2020. Regulation
812 of the RNAPII Pool Is Integral to the DNA Damage Response. *Cell* **180**: 1245-
813 1261.e1221.
814 Tullai JW, Schaffer ME, Mullenbrock S, Sholder G, Kasif S, Cooper GM. 2007.
815 Immediate-Early and Delayed Primary Response Genes Are Distinct in Function
816 and Genomic Architecture. *J Biol Chem* **282**: 23981-23995.
817 Vogt C, Preuss E, Mayer D, Weber F, Schwemmle M, Kochs G. 2008. The interferon
818 antagonist ML protein of thogoto virus targets general transcription factor IIB. *J*
819 *Virol* **82**: 11446-11453.

820 Wang H, Julien O. 2023. CaspSites: A Database and Web Application for
821 Experimentally Observed Human Caspase Substrates Using N-Terminomics. *J*
822 *Proteome Res* **22**: 454-461.
823 Wang Y, Fairley JA, Roberts SG. 2010. Phosphorylation of TFIIB links transcription
824 initiation and termination. *Curr Biol* **20**: 548-553.
825 Watanabe M, Saeki Y, Takahashi H, Ohtake F, Yoshida Y, Kasuga Y, Kondo T, Yaguchi
826 H, Suzuki M, Ishida H et al. 2020. A substrate-trapping strategy to find E3
827 ubiquitin ligase substrates identifies Parkin and TRIM28 targets. *Commun Biol* **3**.
828 Waterhouse AM, Procter JB, Martin DMA, Clamp M, Barton GJ. 2009. Jalview Version
829 2—a multiple sequence alignment editor and analysis workbench. *Bioinformatics*
830 **25**: 1189-1191.
831 Wilson MD, Harreman M, Svejstrup JQ. 2013. Ubiquitylation and degradation of
832 elongating RNA polymerase II: The last resort. *Biochimica et Biophysica Acta*
833 *(BBA) - Gene Regulatory Mechanisms* **1829**: 151-157.
834 Xie Z, Bailey A, Kuleshov MV, Clarke DJB, Evangelista JE, Jenkins SL, Lachmann A,
835 Wojciechowicz ML, Kropiwnicki E, Jagodnik KM et al. 2021. Gene Set
836 Knowledge Discovery with Enrichr. *Current Protocols* **1**.
837 Young AJ, Hay JB, Miyasaka M. 1995. Rapid turnover of the recirculating lymphocyte
838 pool in vivo. *International Immunology* **7**: 1607-1615.
839 Zhang N, Hartig H, Dzhagalov I, Draper D, He YW. 2005. The role of apoptosis in the
840 development and function of T lymphocytes. *Cell Res* **15**: 749-769.
841 Zhang Z, English BP, Grimm JB, Kazane SA, Hu W, Tsai A, Inouye C, You C, Piehler J,
842 Schultz PG et al. 2016. Rapid dynamics of general transcription factor TFIIB
843 binding during preinitiation complex assembly revealed by single-molecule
844 analysis. *Genes Dev* **30**: 2106-2118.
845

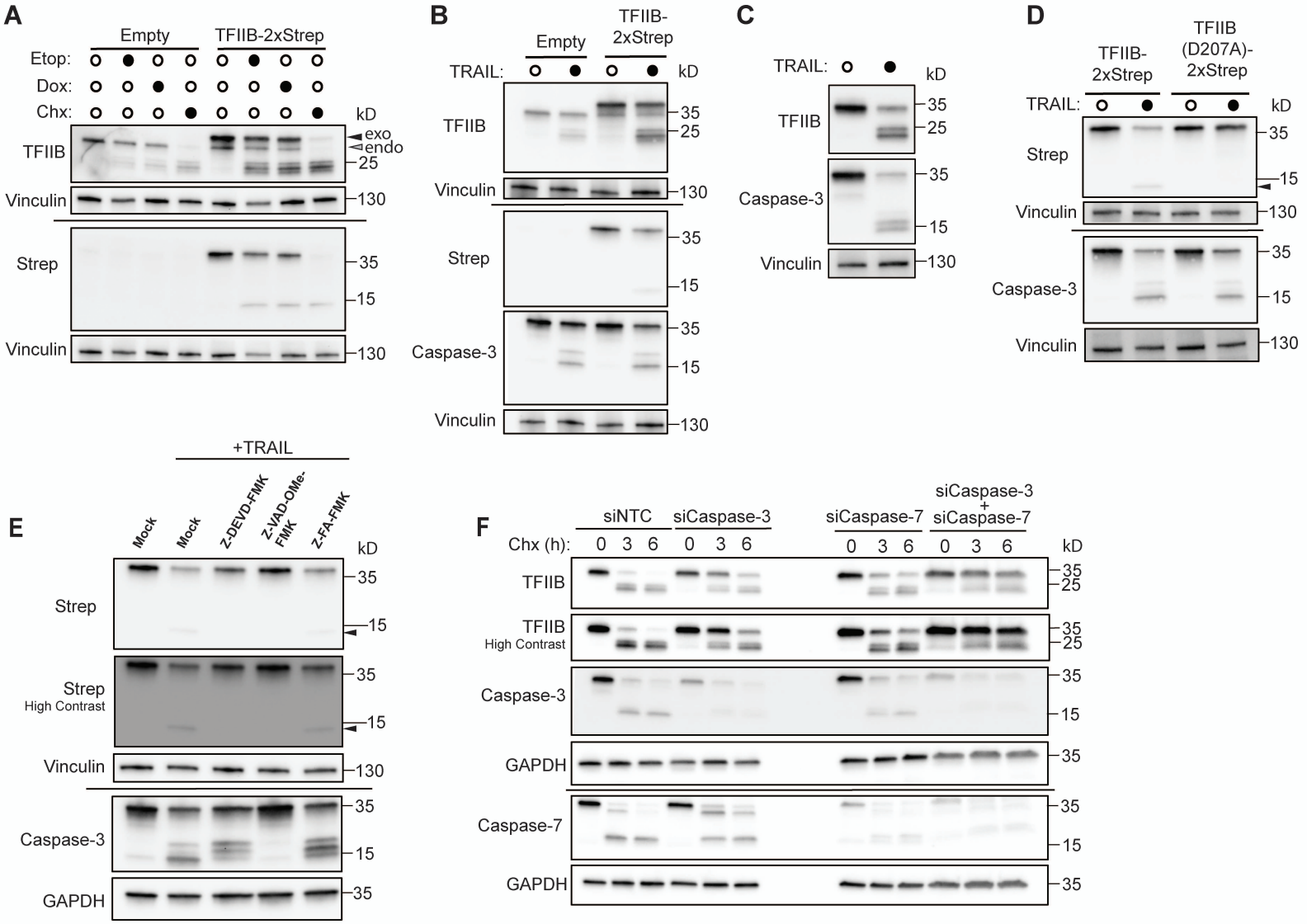

Figure 1. Cellular stress depletes TFIIB via caspase-3/7 cleavage at the D207 residue. (A) BCBL-1 cells expressing the indicated constructs were mock-treated or treated with 25 μM etoposide (Etop) or 2 μg/mL doxycycline (Dox) for 24h, or 100 μg/mL cycloheximide (Chx) for 6 h and analyzed by western blotting. Black arrow indicates full length strep-tagged TFIIB and gray arrow denotes full-length endogenous TFIIB. **(B)** Western blot of BCBL-1 cells expressing the indicated constructs and treated +/- 100 ng/mL TRAIL ligand for 6 h. Caspase-3 cleavage shows induction of cell death. **(C)** Western blot of Jurkat cells +/- 166 ng/mL TRAIL for 6 h. **(D)** As in *(B)* for 8 h. Black arrow indicates cleavage product. **(E)** Western blots of BCBL-1 cells expressing the indicated constructs and treated with 80 μM of the indicated inhibitor for 2 h, followed by treatment +/- 500 ng/mL TRAIL ligand for 7 h. Contrast is enhanced as indicated for visualization of the cleavage product. **(F)** Cells were nucleofected with the indicated control (siNTC) or targeting siRNAs for 48 h followed by treatment with 100 μg/mL Chx for 0, 3, or 6 h and western blotting. Vinculin and GAPDH are loading controls.

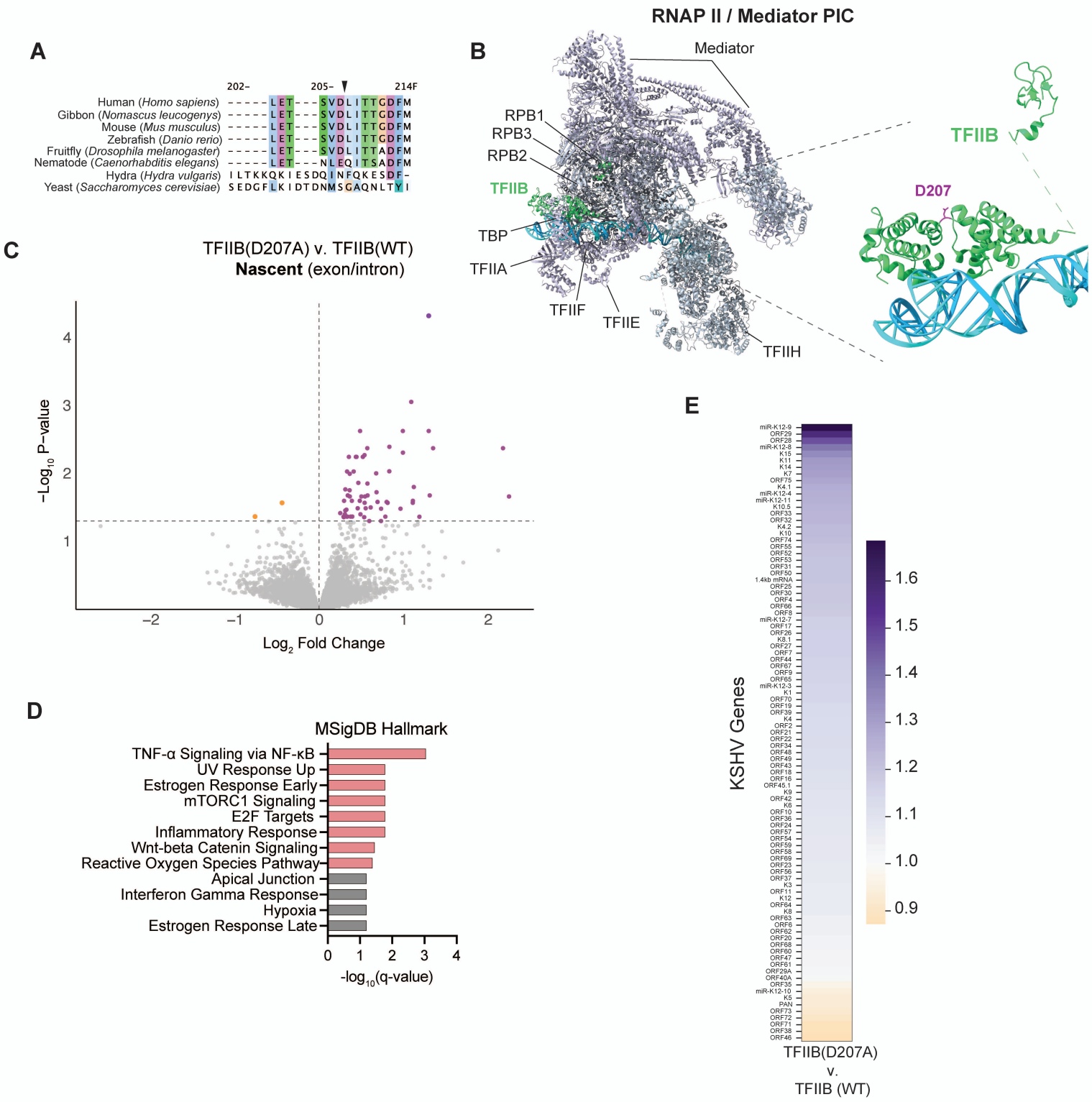

Figure 2. Overexpression of uncleavable TFIIB in apoptosing B cells upregulates some pro-survival genes. (A) Multiple sequence alignment of the TFIIB protein near the D207 locus ranked by evolutionary time. The human sequence is used as a reference with dashes denoting missing areas of homology, and a black arrow indicates the precise location of the caspase cut site. Amino acids are colored with Clustal X scheme in Jalview to represent properties and conservation. **(B)** Structure of the RNAP II / Mediator pre-initiation complex from PDB:7NVR (Aibara et al. 2021) with TFIIB highlighted in green and promoter DNA in blue. Popout: D207 residue is highlighted in magenta between the TFIIB cyclin folds contacting DNA. **(C)** Volcano plot showing differentially expressed genes following exon-intron split analysis from BCBL-1 cells containing TFIIB(D207A)-2xStrep relative to cells containing wild-type TFIIB-2xStrep after 7 h 660 ng/mL TRAIL treatment. Significantly downregulated genes are in yellow and significantly upregulated genes are in purple. **(D)** Molecular Signatures Database Hallmark 2020 (MSigDB) enrichment from annotated genes in TRAIL-specific upregulated nascent RNA from *(C)*. Bars in pink are enrichments with a significant q-value while those in gray have significant p-values but nonsignificant q-values. **(E)** Heatmap of relative gene expression for KSHV genes in TRExRTA BCBL-1 cells expressing either TFIIB-2xStrep or TFIIB(D207A)-2xStrep +/- 24h dox-

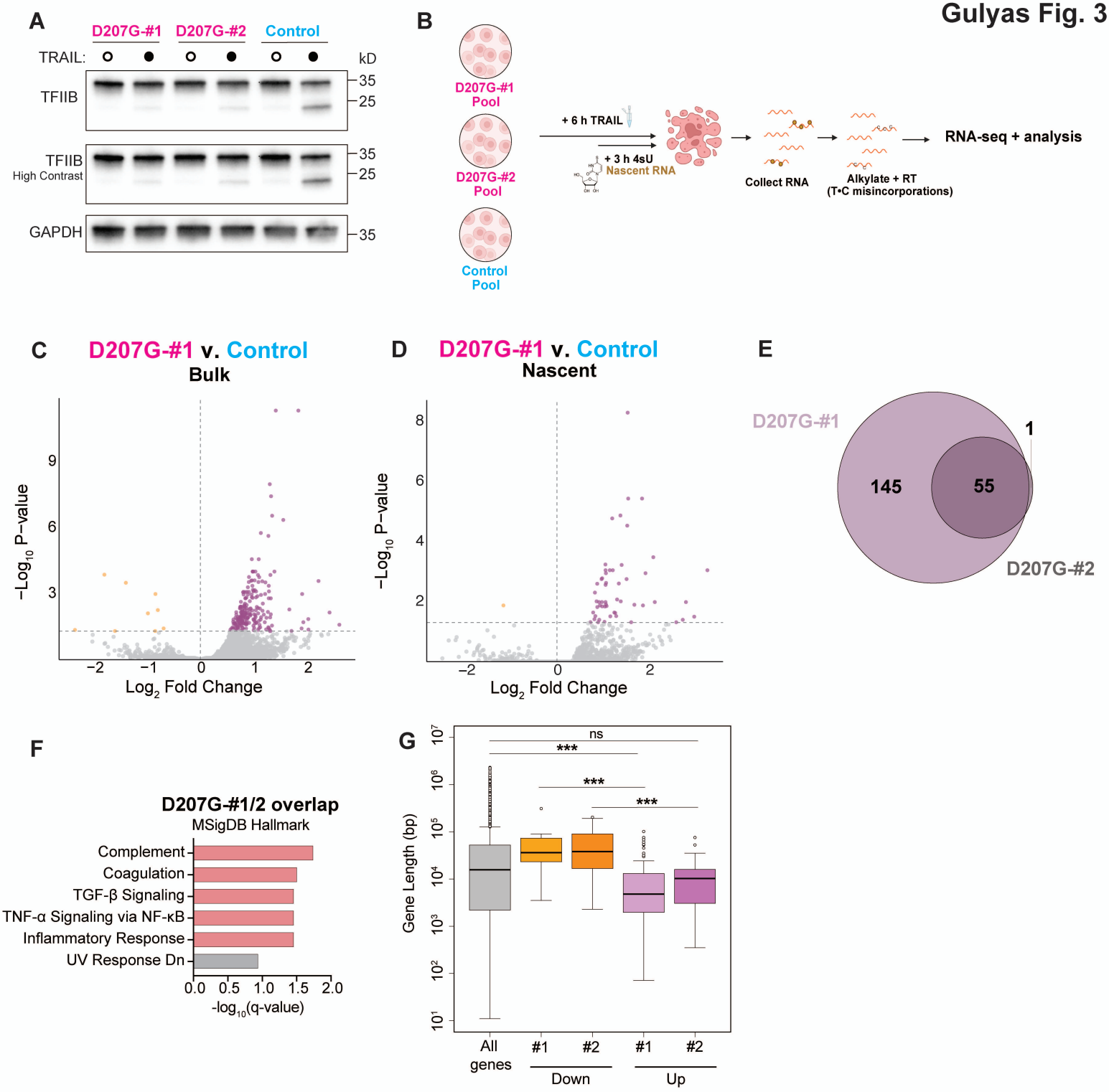

Figure 3. Endogenous TFIIB D207G base editing in T cells dysregulates stress response signaling during apoptosis. **(A)** Western blots of control and D207G based edited Jurkat cell pools following treatment +/- 250 ng/mL TRAIL ligand for 6 h. Contrast is enhanced as indicated and GAPDH is a loading control. **(B)** Schematic for SLAM-seq. **(C-D)** Volcano plot showing bulk *(C)* or nascent *(D)* RNA differential gene expression between the TFIIB D207G-#1 guide and the control guide populations. Significantly downregulated genes are in yellow and significantly upregulated genes are in purple. TRAIL-specific gene upregulations: 200 bulk, 55 nascent. **(E)** Venn diagram overlap of genes upregulated in bulk RNA from D207G-#1 and D207G-#2 versus control guide populations. Genes differentially changed under mock conditions are excluded. **(F)** MSigDB enrichment from the 55 gene overlap in *(E)* with significant q-values in pink and non-significant q- but significant p-values in gray. **(G)** Boxplot comparing gene lengths for all genes detectable in the dataset (n = 23,806) and genes downregulated (yellow) or upregulated (purple) in a TRAIL-specific manner in bulk RNA from D207G-#1 or #2 guide cells. Significance values (Wilcoxon rank sum test with continuity correction) are relative to all genes; ***p < 0.001; n.s. is non-significant (p = 0.089).

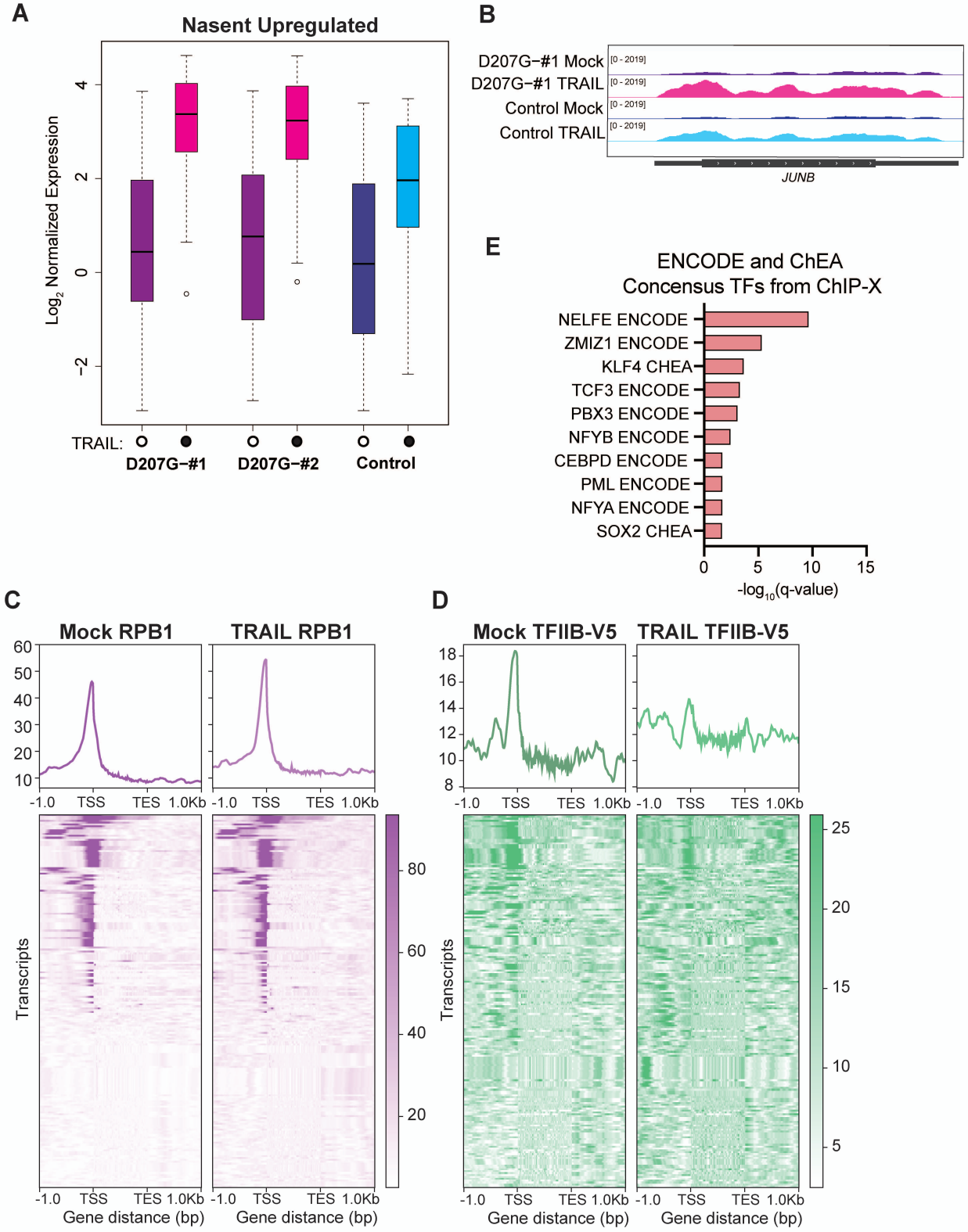

Figure 4. TFIIB-containing pre-initiation complexes are constitutively assembled at the promoters of TFIIB cleavage-sensitive genes. (A) Boxplot showing log2 normalized expression values for the 21 loci nascently upregulated in both D207G-#1 and D207G-#2 pools relative to the control pool during TRAIL treatment. Values are from nascent RNA expression from SLAM-seq analysis. **(B)** Bulk RNA coverage track of *JUNB* in D207G-#1 or control cells during mock or TRAIL-treatment. **(C-D)** Metagene plot heatmaps and profiles for ChIP-seq signal of RPB1 *(C)* and TFIIB-V5 *(D)* at these transcript coordinates (n = 197). TSS = transcription start site, TES= transcription end site; kilobases plotted up and downstream are indicated. **(E)** Enrichment for transcription factors targeting genes nascently upregulated from TRAIL-treated TFIIB(D207A)-expressing BCBL-1 cells, clonal D207G Jurkat cells, or in the D207G-#1 and D207G-#2 Jurkat pool overlap relative to their respective controls was assessed with ENCODE and ChEA Consensus Transcription Factor sites from ChIP-X. All q-values are significant.

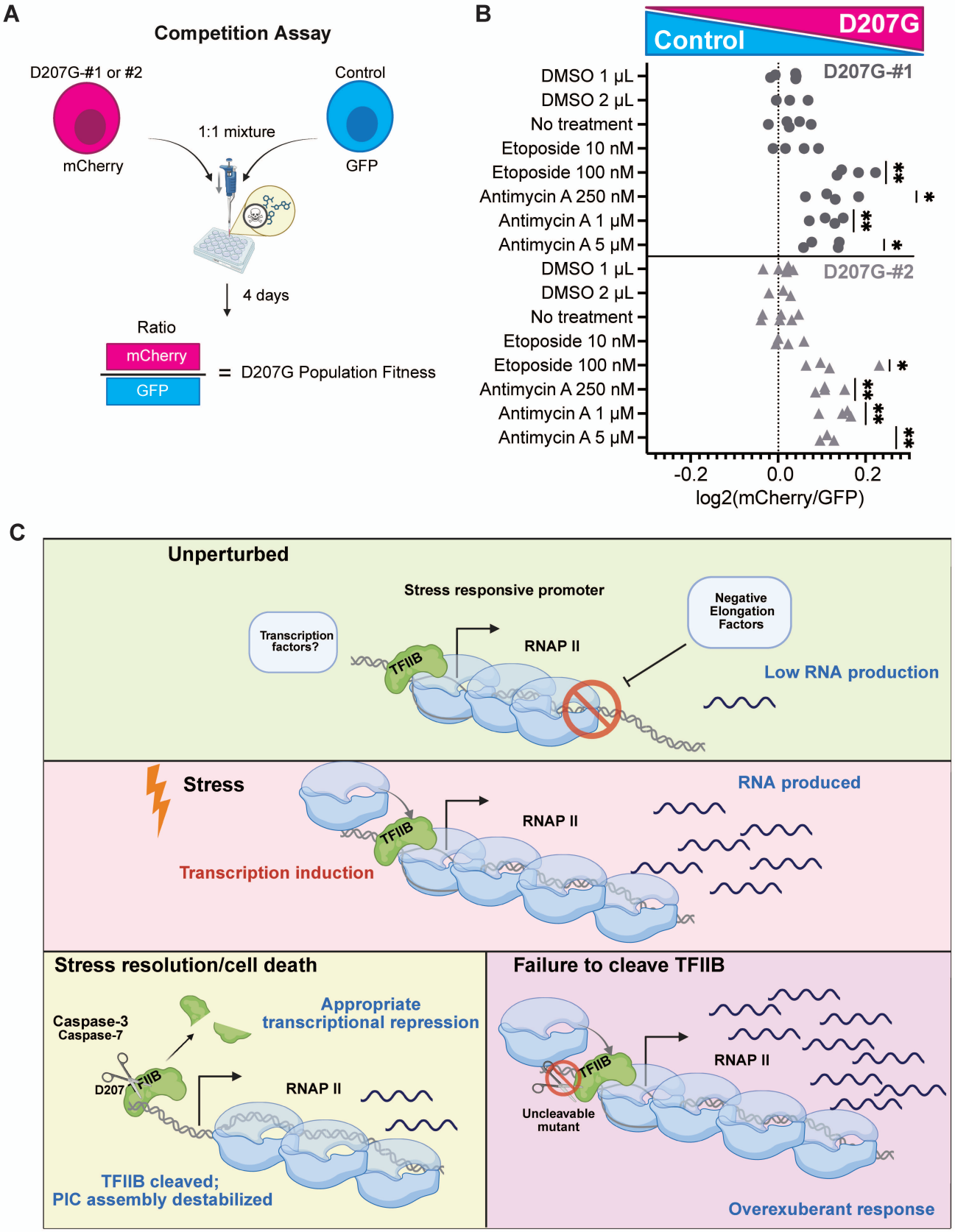

Figure 5. TFIIB D207G cells outcompete control cells in co-culture during chemical stress.
(A) Schematic of the cell growth competition assay. Fluorescence measurements quantifying the relative percentage of mCherry and GFP cells were made via flow cytometry. Differences in plating and basal growth were accounted for by normalizing mCherry:GFP ratios to that of a DMSO control measured on Day 3. **(B)** Log_2 normalized mCherry:GFP ratios for independent replicates of D207G-#1:control competitions (circles) and D207G-#2:control competitions (triangles). *$p < 0.05$, **$p < 0.01$; one sample t-test with theoretical mean of 0. **(C)** Schematic of model hypothesizing how TFIIB occupancy and cleavage regulate stress-responsive genes.